

Fast and accurate Zero-defect manufacturing using collaborative real-time photogrammetry

Francesco Messina¹, Andrea Maria Lingua^{2*}, Alessio Martino², Francesca Matrone², Paolo Maschio²

¹ Department of Electronics and Telecommunications (DET), PoliTO Interdepartmental Centre for Service Robotics (PIC4SeR); Politecnico di Torino, Corso Ferrucci 112, 10138, Italy – francesco_messina@polito.it

² Department of Environment, Land and Infrastructure Engineering (DIATI); Politecnico di Torino, Corso Duca degli Abruzzi 24, 10129, Italy – (andrea.lingua, alessio.martino, francesca.matrone, paolo.maschio)@polito.it

Keywords: Real-time photogrammetry, industrial metrology, Zero-Defect manufacturing, augmented reality

Abstract

For the machining of industrial components, their accurate alignment on operative machines is a crucial step with significant impacts on the whole process, especially when dealing with large-scale elements. To achieve this alignment, a trained operator is needed along with expensive equipment, such as laser trackers, whose correct use requires the measurements of many significant points and is time-consuming. The lack of a precise alignment comes with possible incorrect parts machining, resulting in quality concerns and potentially expensive rework. To face this problem, collaborative real-time photogrammetry is an effective solution for guiding untrained users in correctly positioning various measured and codified components to generate the best solution for machining high-volume parts. The solution proposed in this contribution is part of the TACCO project, co-financed by EIT Manufacturing (co-funded by the EU). It takes advantage of the TACCO system, where auxiliary components (scale bars, dome-shaped components, coded targets and a cross-reference system) are placed on the object to be measured for their correct positioning in order to obtain an optimal photogrammetric reconstruction. This allows the reduction of the error ellipsoids on several uncoded targets, which are calculated through an iterative simulation carried out in a MATLAB environment. Unskilled operators are then guided through an Augmented Reality headset for their correct placement on the real-world object and for defining the positions and orientations from which to acquire images. This methodology will lead to an accurate measurement of the target points to be machined and, thus, a precise alignment process for the subsequent machining operations.

1. Introduction

Metrology is fundamental in the industrial field, especially when working with components of large dimensions. These elements are utilized in critical applications for relevant sectors such as Aerospace and Shipbuilding, as well as Energy and Transportation Infrastructures. Raw pieces deployed in these industrial fields can easily reach linear dimensions of tens of meters and require high-level accuracy when machined. Their use in such primary and relevant areas requires careful planning of every step, which makes up for their assembly and refinement. Large Volume Metrology (LVM) is crucial in ensuring that the elements or parts on which milling operations must be carried out are accurately measured and correctly positioned on the working machine.

The current state-of-the-art for LVM includes the employment of expensive equipment such as Coordinate Measuring Machines (CMMs) or laser trackers, which provide high-level accuracy but, at the same time, require significant financial investments, dedicated facilities, trained personnel, and, more importantly, a considerable amount of time. An effective solution to this series of challenges can be found in the technique of Photogrammetry, which is the process of obtaining reliable and precise measurements from images (Bösemann, W., 2005; Wang, Q. et al, 2013; Galantucci, L.M. et al., 2016). Using high-resolution cameras and dedicated algorithms (Girelli et al., 2022), it is possible to accurately reconstruct three-dimensional models of an industrial component by acquiring multiple images of the aforementioned object, without requiring highly trained or skilled operators and in a relatively short time. Photogrammetry specifically beneficial for the accurate reconstruction of massive components without the use of cranes, mechanical arms or ladders, once again reducing costs, time and most importantly risks for human operators. The costs of high-resolution cameras and commercial software used for photogrammetric

reconstruction are, in fact, negligible compared to those of a laser tracker or a CMMs, significantly lowering the amount of money needed for the metrological control in the industrial pipeline.

1.1 TACCO Project

This contribution addresses a part of the *TACCO project for the fast and accurate zero-defect part set-up*, composed of three modules:

- M1 - Measuring with real-time interactive photogrammetry (explained in this contribution),
- M2 - Fitting
- M3 - Alignment.

The goal of the project is to develop, by the end of 2024, an attractive and user-friendly *Human Machine Interface* (HMI) to guide inexperienced operators for the LVM of industrial components. The final objective of modules M1 + M2 is to handle components with dimensions of up to 30 meters and a relative accuracy towards 1:100.000. The project is co-financed by the European Union, specifically in the framework of the *European Institute of Innovation and Technology (EIT) Manufacturing*, with partners located in different European countries. It is considered an improvement of the VSET System (Mendikute et al., 2017), which takes advantage of calibrated, codified, and retroreflective auxiliary elements (Figure 1) for the accurate acquisition of the position of points to be machined.

1.2 Related works

The precise measurement of industrial components using the non-contact technique of photogrammetry has been studied for many years, with the definition of state-of-the-art industrial photogrammetry (Fraser, 1993) also covering those large-volume components, but with the limitations of a tedious film measurement stage. The impact of computer vision through the

last decades has significantly helped reduce the elapsed time for both the camera calibration and the data processing phase in high-accuracy photogrammetry (Remondino & Fraser, 2005; Balletti et al., 2014).

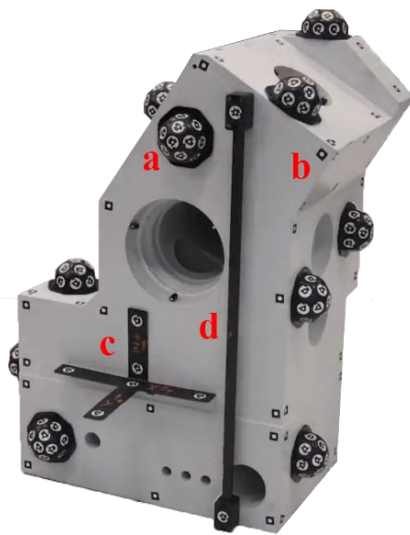


Figure 1. Example of a raw component with the additional elements placed on its surface: a) Dome-shaped auxiliary elements b) Uncoded target where machining has to be carried out; c) Cross Reference System (CRS); d) Calibrated scale bar.

This happened thanks to techniques of automated self-calibration, which include sensor modelling via both targeted arrays and targetless scenarios, enhancing the processes employed for close-range photogrammetry (Luhmann, Fraser & Maas, 2015). The simultaneous calibration and orientation assessment of multi-camera 3D measurement systems for LVM has also been conducted by using additional elements such as scale bars positioned around the volume and conducting self-calibrating bundle adjustments (Luhmann, 2010; Franceschini et al., 2014; Sun et al., 2018; Sun et al., 2019).

The use of these components, along with optical targets placed on the object for reconstructing their accurate position via close-range photogrammetry, has had a crucial role in measuring large-volume raw parts that must be machined with high-level precisions. (Puerto et al., 2022). Through the calibration and orientation of multi-camera systems for LVM, it is possible to highly increase accuracy, reaching levels of precision that come close to those of a laser tracker (LT), which also makes use of spherically mounted retroreflectors (SMRs) to achieve low measurement uncertainties for large volumes, but with a much smaller financial impact and with increased levels of automation, reducing the need of human intervention (Leizea et al., 2023). In this paper, the authors propose a procedure for assisting untrained operators in reaching relative accuracies towards 1/100.000 via an iterative simulation that takes advantage of pre-calibrated scale bars, codified and uncodified optical target to obtain their best placement on the object, along with the definition of the camera pose for the photogrammetric acquisition.

2. Methodology

To reach accuracies towards 1:100.000 with a photogrammetric approach, a user-friendly HMI and workflow must be defined to assist untrained personnel in positioning the pre-calibrated and

codified auxiliary elements. These components will be fundamental in the scene reconstruction and, consequently, in the detection of target points to be machined (uncoded target - UT). To guide the user through the measurement process, while simultaneously increasing the quality and precision of the measurements made through photogrammetry, a methodology was devised to estimate the error of ellipsoids belonging to each uncoded target, according to predetermined user-selectable acquisition strategies. The simulations' inputs are essentially three:

- a properly designed .STL format object file of the industrial component,
- the relative locations of the uncoded target points to be machined, and
- a configurable external parameter table that defines every other aspect of the simulation.

With all these elements, it is possible to recreate the different phases an operator would have to carry out to accomplish the measurement, but automatically and iteratively to reach an optimal solution. The simulation output is a list of the best-defined positions of each auxiliary element of the implemented VSET, the TACCO system, along with the camera poses, which are the positions and orientations from which the images must be acquired to achieve an optimal result. Once all these positions are obtained, they are passed as STL format object files to the augmented reality viewer, which allows the operator to visualize precisely where each auxiliary element (cross reference system, calibrated scale bars, auxiliary coded target) has to be placed on the real-world geometry of the object to be machined. Finally, the user is guided in the image acquisition process, with a camera wirelessly connected to a PC for the ultimate reconstruction of the true and accurate location of the UTs with respect to the desired object. The following chart (Figure 2) summarizes the proposed pipeline of the authors' work.

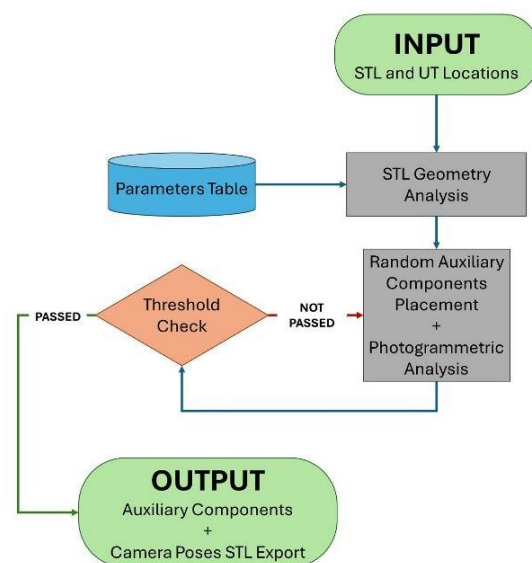


Figure 2. Methodological pipeline

2.1 Random object generation and camera pose definition

At the beginning of the simulation, the first step is the identification of the surfaces of the object on which the auxiliary components of the TACCO system can be placed. Once the STL of the object is loaded, it is meshed as finely as possible to achieve a high number of mesh nodes while keeping it computationally light. The normal vectors of each node are then calculated, from which a single normal for each planar face is

determined to properly rotate each component and place it in the correct direction. The second step is positioning the UTs, whose relative locations are known a priori and provided by the user on the surfaces to be machined. These positions are then excluded from the list of possible nodes where the auxiliary components of the TACCO system can be placed.

From the aforementioned process, a list of available positions for each planar face of the model is computed according to the geometrical constraint of the different auxiliary elements to be placed. Based on the maximum number of available auxiliary elements of each type some random positions are selected from random faces and elements are virtually placed on those positions, checking each iteration for possible collisions. The different types of elements inside this loop are placed in a predefined order, first Cross Reference, then the Scale Bars, and lastly, the Dome-Shaped auxiliary components, based on the element relevance for the final computation of the ellipsoids error. An example of the result of this process is shown in Figure 3.

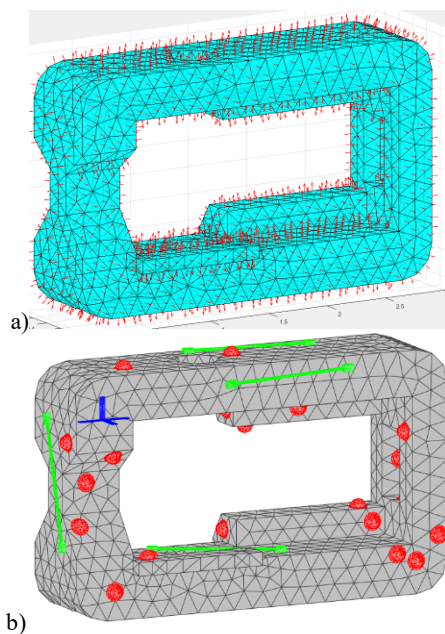


Figure 3. Example of visualization of the normal vectors on the finely meshed object (a) and Positioning of the auxiliary elements (b).

Once all the auxiliary components have been randomly positioned with no collision, the following step is the generation and definition of the camera poses according to the strategy chosen by the user. Three possible strategies have been selected: Spherical, Ellipsoidal, and Buffer (Figure 4), with the purpose of defining the best based on the object's geometry and the available space around it. The first acquisition strategy is based on generating a series of circular trajectories, forming a kind of hemisphere along the Z axis centered around the barycentre of the component to be analyzed. The second one is based on the generation of a series of ellipsoidal trajectories in which the two foci fall within the major axis of the component, forming an ellipsoid developing along the Z axis. Finally, the third strategy has trajectories following the contour of the element at a fixed distance, as if they were offsets from the component, generated every few meters along the Z-axis in relation to the element's height. An example of camera pose generation using this last strategy can be seen in Figure 5.

Once all the camera positions are calculated based on the chosen strategy, there is a phase in which the error of each ellipsoid on the UT is calculated and compared to a user-selected threshold value, that defines the maximum admissible error for that measurement. This whole process is performed inside an outer loop where the random positions of auxiliary elements are recomputed until the above-mentioned threshold constraint is verified. When the maximum error falls within the selected threshold, the positions of the auxiliary elements, along with the camera poses, are saved and exported to be passed to the VR system. The duration of the simulation varies depending on several factors, including the size of the mesh and the number of available surfaces, the maximum number of auxiliary components to be positioned on the piece, the number of attempted runs of the simulation and the number of cores of the machine on which it is performed.

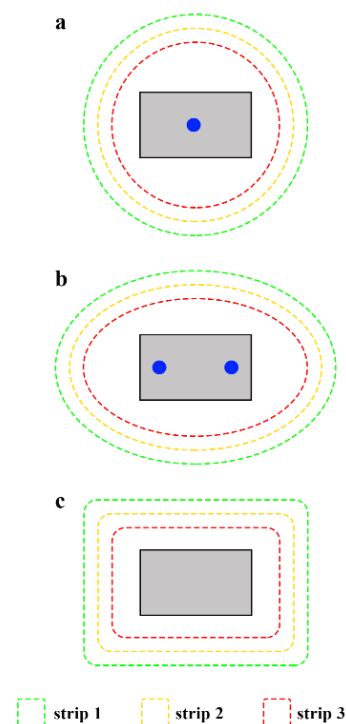


Figure 4. A top-view schema of the three implemented strategies: spherical (a), ellipsoidal (b), and buffer (c).

2.2 Montecarlo approach using Least Square Simulation

One of the main issues highlighted by end-user partners who provided feedback and who had already tested the VSET system, was the methodology for positioning the auxiliary components, which was done randomly, and their distribution on the object greatly affected uncertainty. For this reason, a system design has been developed to assist the end-user, which includes the estimation of the best locations for the auxiliary elements (coordinate system bar, scale bars, dome-shaped components), as well as the number and poses of the images. In fact, another problem they encountered was that beyond a certain number of photos the system started slowing down in processing and calculation due to a bottleneck in the system.

In the paper is to maximize the result (i.e. minimize the error of the ellipsoids) by reducing the number of images necessary to achieve the desired accuracy. These parameters are defined based on the accuracy and precision requirements of the TACCO

system (a minimum admissible semiaxis of error ellipsoid λ_{adm}), fixed by the user to develop the specific industrial application to reduce the number of components and required images.

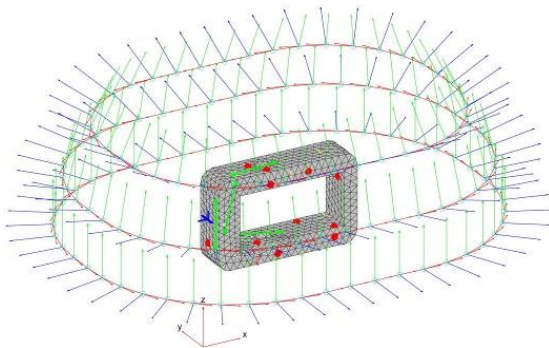


Figure 5. An example of camera pose generation using the Buffer Acquisition strategy.

Therefore, another of the objectives of the methodology proposed To solve this complex problem, a Monte Carlo approach has been proposed, which will be deeply explained in a following detailed contribution. The optimal solution can be found by minimizing a cost function that summarizes numerous analytical parameters connected with the requirement of the measurement system.

2.3 Least square simulation of bundle block adjustment

In the design phase of the measurement system, there are no available measures; then it is not possible to use real data: we thus need to develop a solution without real measurement, using a simulation approach. The algorithm used to obtain photogrammetric measures is the bundle block adjustment, which can be simulated (as all the least square adjustment problems) without the need for actual measurement by choosing:

- a correct definition of reference system and other constraints (location of reference system bar and scale bars);
- a real proposition of photogrammetric measurements according to the specific application (3D model of the raw component, uncoded targets, igloos, characteristics of the digital camera of the TACCO system);
- a realistic hypothesis on the average measurement precision. This parameter is defined "a priori" before the adjustment as the standard deviation of measures and constraints: precision of scale bar length $\sigma_{SB} = 0.1$ mm, precision of coordinates of reference system bar $\sigma_{RS} = 0.05$ mm, precision of measured image coordinates $\sigma_I = p \cdot d_{pixel}$ (a fraction of the pixel size $p = 0.2-1$ pixel), "a priori" precision of unit weight $\sigma_0 = 1$ mm.

Under the hypothesis that there are no measures with blunders or outliers, it is possible to assume that the "a priori" deviation is a good approximation of the "a posteriori" one: this consideration makes it possible to simulate the solution of the LSM adjustment from the point of view of precision estimation.

Supposing the analytical model of collinearity equations, the characteristics of a digital camera, such as the focal length, pixel size and sensor size, the geometry of the measurement systems with the location of coordinate system bar, scale bars, igloos and uncoded points and the location and rotation of images (randomly defined in Monte Carlo approach), it is possible to compile the design matrix A (also known as coefficient matrix, model matrix or regressor matrix) of the simulated least squares method (LSM) of photogrammetric bundle block adjustment:

$$AX = T + v \quad (1)$$

where T is the column vector of the measures (known terms), X is the column vector of unknowns, and v is the column vector of residuals.

Without real measures, it is not possible to evaluate the known term T and solve the LSM, but the normal matrix $N = A^T P A$ can be calculated using the weight matrix P (according to the "a priori" precisions of measures).

The inverse normal matrix N^{-1} is estimated using the Monroe-Penrose pseudo-inverse (Monroe, 1920, Penrose, 1955) based on singular value decomposition (SVD) to prevent ill-conditioned problems of the equation system.

The hypothesis of "a priori" σ_0^2 permits the estimation of covariance matrix of unknowns:

$$C_{xx} = \sigma_0^2 N^{-1} = \begin{pmatrix} \dots & \dots & \dots & \dots & \dots \\ \dots & \sigma_{X_i}^2 & \sigma_{X_i Y_i} & \sigma_{X_i Z_i} & \dots \\ \dots & \dots & \sigma_{Y_i}^2 & \sigma_{Y_i Z_i} & \dots \\ \dots & \dots & \dots & \sigma_{Z_i}^2 & \dots \\ \dots & \dots & \dots & \dots & \dots \end{pmatrix} \quad (2)$$

In a photogrammetric bundle block adjustment, a part of the solution is a set of 3D coordinates of uncoded targets where the TACCO system needs to guarantee the correct precision, then in the covariance matrix, the relative position contains variance/covariance values on these i -th 3D uncoded points (highlighted in the red block in the previous equation). The eigenvalues and eigenvectors of this sub-covariance matrix are then used to calculate the size, shape and orientation of the 3D error ellipsoid representing the precision of the estimated 3D coordinates $P_i = (X_i, Y_i, Z_i)^T$ of i -th uncoded point. Rigorously, the error ellipsoid represents an iso-surface of the 3D Gaussian distribution, and allows the visualization of a 3D confidence interval with a specific level of confidence: generally, a confidence level of 95% is used, then in this case, the error ellipse defines the region that contains the 95% of all possible points that can be drawn from the underlying Gaussian distribution.

The cost function is defined using the max semiaxis of the obtained ellipsoids of uncoded targets (λ_{max}) which is selected and stored for guiding the Montecarlo iterative solutions, searching the minimum value:

$$\min(|\lambda_{max} - \lambda_{adm}|) \quad (3)$$

Using the previously defined matrixes, the redundancy matrix R can be determined using:

$$R = I - AN^{-1}A^T P \quad (4)$$

In the main diagonal, the redundancy matrix contains the values of the local redundancy of each measure. This local redundancy r_i for the i -th measure is limited in the range $[0, 1]$ and explains how is the influence of the i -th measure in the whole LSM adjustment.

The redundant matrix is estimated to prevent solution with too small redundancy with small value of semiaxis of error ellipsoids. With this simulation, it is possible to design the whole system, allowing for the definition of an optimized cost function without any actual measurement.

2.4 Procedure based on design orders

To do so, a sequential workflow has been defined, inspired by the level order design of the geodetic network using least square simulation, where each step fixes a part of the final design:

- the *zero order design* (ZOD) permits to define the best location of reference system bar, located in the part of surface of raw component close to the centroid. At the end of this step, the location of reference system bar is fixed;
- the *first order design* (FOD) is devoted to the definition of number and location of scale bars and igloos, starting from an hypothesis of image poses with high values of horizontal (80%) and vertical (60%) overlapping. The procedure chooses the best solution according to the cost function (3);
- the *second order design* (SOD) is applied with different image pose schema (previous Figure 5) varying horizontal (60-80%) and vertical (40-60%) overlapping to simplify the photogrammetric block.

Within the simulation, all the intrinsic parameters of the camera that will be later involved in the actual measurements are defined. Each target available in the scenario (uncoded targets, CSR, extremes of scale bars, and dome-shaped auxiliary elements) is checked in each image whether it is "included and visible", and two equations are written for each point. Figure 6 shows an example of an optimal solution in which the errors computed on the ellipsoids are really small, with a magnification scale of 1000.

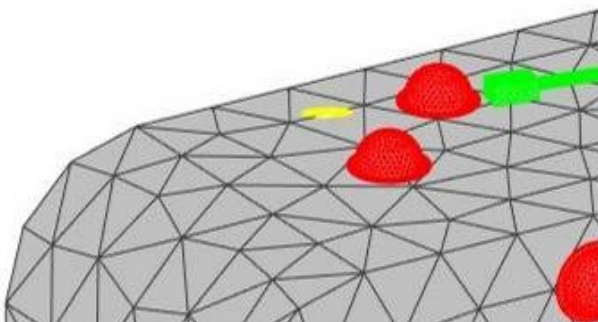


Figure 6. Example of an optimal solution and error ellipsoid around an uncoded target with a magnification scale (yellow).

2.5 Final solution implementation in an AR viewer for user guidance

To assist inexperienced operators in acquiring images with the correct camera pose, a system has been devised to guide them toward suitable positions virtually. After evaluating different strategies between mobile phone apps and Augmented Reality devices, the latter one has been chosen, for which the most popular off-the-shelf and commercial AR viewers have been analysed, ultimately identifying in PICO 4 (Figure 7) the solution for the TACCO project, being cost-effective compared to others while at the same time providing the best resolution as can be seen in Table 1.

	Resolution	Refresh rate (Hz)	FOV	Storage	Price (*)
<i>Meta Quest 2</i>	1832x1920	60/72/90	97°	128/256 GB	400 € 450 €
<i>PICO 4</i>	2160x2160	72/90	105°	8 GB + 128/256 GB	380 € 430 €
<i>Vive XR Elite</i>	1920x1920	90	110°	12 GB + 128 GB	1.100 €

Table 1. Specifications of the main available VR solutions
 (*) Prices updated to May 2023.

With this device, the operator can visualize at the same time the real world with the manufactured piece and the virtual models coming from the simulation jointly with the best auxiliary elements location and camera poses for the TACCO System acquisition process. Three STL files generated from the simulation are needed: one that defines the geometry of the object to be machined, the TACCO system auxiliary components (cross reference system, scale bars, and dome-shaped elements) best positioned on the object, and finally, the well-determined camera poses around the object.



Figure 7. PICO 4 AR System

Among the different applications available, a free-to-use app whose primary purpose is digital 3D drawing called Gravity Sketch has been chosen. It offers many valuable tools, such as measuring, dividing elements into layers, and managing each element aspect by tuning its colour, transparency, and visibility. Most importantly, it allows the user to seamlessly switch from the VR environment of a white canvas with the STL models to an AR environment, perfectly combining the real and the virtual model. In the proposed workflow, once the models are exported from MATLAB and uploaded into the AR device via PC through the app managing site, the user can freely adjust the appearance and visibility of every element for each layer. The virtual model (Figure 8) can be roto-translated until it perfectly overlaps its real-world counterpart. The object model can then be turned off, allowing the operator to precisely place the auxiliary elements on the object and acquire the correct camera poses, depicted as spheres from where to capture each image.

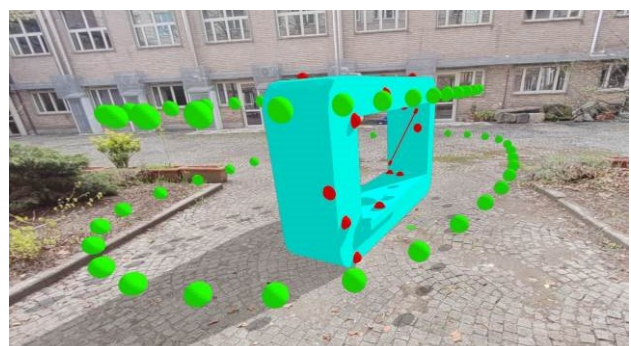


Figure 8. Virtual model of the component to be machined (light blue), auxiliary elements (red), and camera poses (green).

Another interesting possibility to help the operator capture photos from the correct perspective is to show the user in the VR environment, at each camera pose, a synthetic image corresponding to the correct viewpoint from which to take the photo. These images are generated at the end of the simulation using some MATLAB toolboxes that let you create a synthetic environment in Unreal Engine in which you can place each model and auxiliary component with its real texture and simulate the acquisition phase. An example of a synthetic image created with this method is shown in Figure 9.

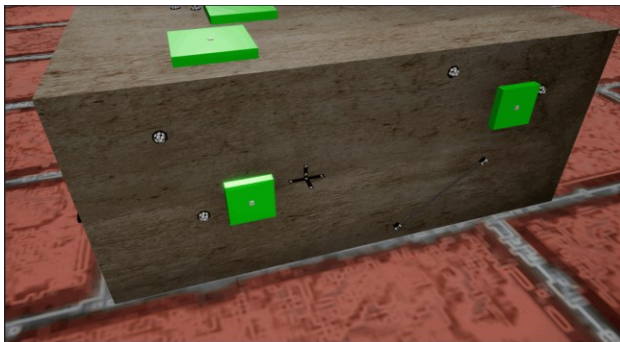


Figure 9. Example of synthetic image generated in Unreal Engine.

3. First result and validation

The proposed methodology was applied to simple blocks of various sizes to verify the applicability of the TACCO system in different scenarios.

For each case, a set of 100 simulations was realized, defining the values summarized in Table 1, and highlighting the following results:

- the minimum number of scale bars for a good solution is 4, also for relatively small objects;
- with 5-6 scale bars, the simulation shows that the TACCO system can solve the problem for large raw components (< 30 m) with a precision (95 %) of 0.3 mm, equivalent to about 1:90000;
- the solutions are not heavily influenced by the number of igloos that can change from 5 to 15 without significant impacts;
- the number of images grows for large sizes of raw components to guarantee a high level of precision;
- with the implemented schema of the photogrammetric block (buffer, spherical, ellipsoidal), the local redundancy of the UT is usually greater than 0.5 with mean values of 0.8: the solution estimated is not affected by poor redundancy in UT coordinates estimation;
- the multiplicity is always high, varying in the range of 15-25, with a mean value of 20: the solutions are controllable and reliable;
- good results are obtained with distances from objects and images in the 4-8 m range.

Block dimensions $\Delta X, \Delta Y, \Delta Z$ [m]	N. of scale bars	N. of Igloos	N. of images	Max Semiaxis (95%) [mm]	Mean Red. UT
3x2x1	4	5-10	35-65	0.19	0.82
5x3x1.5	4	5-10	37-78	0.23	0.75
10x4x2	4	6-12	43-88	0.26	0.82
20x5x2	5	6-12	52-130	0.29	0.85
30x10x2	6	7-15	63-160	0.33	0.91

Table 1. Summary of first results.

To verify the goodness of the above-mentioned methodology, a comparison of the estimated precision has been done using the Fraser empirical formulas:

$$\sigma_{XYZ} = \frac{qD}{c\sqrt{k}} \sigma_i \quad (5)$$

where:

- k is the mean number of images with the same point (multiplicity).

- q is the shape factor (0.4-0.8), which describes the goodness of the configuration of spatial resection between images and is generally connected with the angles between intersecting homologous rays;
- D is the mean distance between images and points;
- c is the focal length;
- σ_i is the precision of the measured image coordinates, 0.5 pixel size in this case.

The solution is simulated using the intrinsic parameters of the digital camera: Nikon Z6 II, 24.3 MP, 6048x4024 pixels, pixel size of 5.94 μm , lens Nikkor Z 35mm. In Table , it is shown that the estimated precision is comparable to the one evaluated with the empirical formula of Fraser, confirming the goodness of the simulations.

K	q	4	8	D [m]
		111	222	D/c
20	0.4	0.17	0.34	mm
20	0.6	0.25	0.51	mm
20	0.8	0.34	0.68	mm

Table 2. The estimated σ_{XYZ} using the Fraser formula and the camera Nikon Z6 II, lens Nikkor Z 35mm.

The proposed methodology will be improved, tested, and validated using a precise and accurate laser tracker: the Leica Absolute Tracker AT403 (Figure 11), capable of continuous measurements and reflector tracking features. It is used in industrial settings for large-scale metrology and quality control. The AT403 boasts a maximum measurement range of 320 meters, with an accuracy of up to 10 microns, thanks to its advanced Absolute Interferometer technology. It can operate in various environmental conditions, such as extreme temperatures and vibration, without affecting the accuracy of the measurements.



Figure 10. The Leica Absolute Tracker AT403

Validation will be carried out using a laser tracker as the ground truth measuring instrument to assess the goodness of the simulation in two different scenarios. For medium-sized objects (between 5 and 15 meters of linear length), the validation phase will be carried out by using a car since it satisfies different aspects

for the validation phase of the TACCO project: magnetic external elements can be firmly positioned on it with ease, it can be freely moved in an open environment, and virtual models can easily be found online. For bigger-sized objects (from 15 to 30 meters in dimensions), the tests will be carried out in one of the partner's facilities since similar-sized objects are already available, as well as a laser tracker.

SPECIFICATIONS	
Accuracy (Absolute Distance Performance)	$\pm 10 \mu\text{m}$ ($\pm 0.00039''$)
Accuracy (Absolute Angular Performance)	$\pm 15 \mu\text{m} + 6 \mu\text{m/m}$
Operating temperature	-15°C to $+45^{\circ}\text{C}$
Laser Safety	Class 2 Laser Product in accordance with the IEC 60825-1 Second Edition (2014-05)
Range	Up to 320 m

Figure 11. Leica Absolute Tracker AT403 and its specifications.

4. Conclusions

The methodology devised in the TACCO Project aims towards the relative accuracy of 1:100.000 while simultaneously creating a relatively low-cost and easy-to-use system for untrained operators to position the elements around the object to be machined and acquire images through a collaborative approach. The simulations carried out so far showed that using the level order design, it is possible to reach a very high level of accuracy, and once validated with actual measurements using laser trackers, a new milestone in close-range photogrammetry for industrial metrology could be set.

Acknowledgements

The TACCO Project (tacco-project.eu) is funded by the EIT Manufacturing (co-funded by European Union) and among the partners (Ideko, Mondragon, Soraluce, Renishaw Iberica, Officine Meccaniche B.B.M., Maschinenfabrik Wüstwillenroth GmbH, Dr. Matzat) can be found different realities such as milling machine construction companies, probing and gauging system experts, fixtures and clamping elements designing companies, as well as end-user manufacturing companies producing large-volume components, research centre and universities. The contribution of the Politecnico di Torino research team is to improve the user experience and the overall accuracy of the target points to be machined positioning, refining the work done by partners on VSET for reaching new milestones in the use of Photogrammetry for Industrial Alignment.

References

Balletti, C., Guerra, F., Tsioukas, V., and Vernier, P. (2014). Calibration of Action Cameras for Photogrammetric Purposes. *Sensors* 2014, 14(9), 17471-17490. <https://doi.org/10.3390/s140917471>

Bösemann, W. (2005). Advances in photogrammetric measurements solutions. *Computer in Industry*. Volume 56, Issues 8-9, 886-893. <https://doi.org/10.1016/j.compind.2005.05.014>

Franceschini, F., Galetto, M., Maisano, D., and Mastrogiacomo, L. (2014) Large-scale dimensional metrology (LSDM) from tapes and theodolites to multi-sensor systems. *International Journal of Precision Engineering and Manufacturing*. Volume 15, 1739-1758. <https://doi.org/10.1007/s12541-014-0527-2>

Fraser, C.S., (1988). State of the art in industrial photogrammetry. *Proceedings of the ISPRS Congress of Kyoto 1988*, Volume XXVII, 166-181

Galantucci, L.M., Pesce, M., and Lavecchia, F. (2016). A powerful scanning methodology for 3D measurements of small parts with complex surfaces and sub millimeter-sized features, based on close range photogrammetry. *Precision Engineering*, Volume 43, 211-219. <https://doi.org/10.1016/j.precisioneng.2015.07.010>

Girelli, V. A., Tini, M. A., and Bitelli, G.: Very high-resolution 3d surveying and modelling experiences in civil engineering applications, *Int. Arch. Photogramm. Remote Sens. Spatial Inf. Sci.*, XLIII-B2-2022, 673–678, <https://doi.org/10.5194/isprs-archives-XLIII-B2-2022-673-2022, 2022>.

Gurturk, M., Masiero, A., Toth, C., Dabove, P., Di Pietra, V., Vettore, A., Guarnieri, A., Cortesi, I., Pellis, E., and Soycan, M.: A Test On Collaborative Vision And UWB-Based Positioning, *Int. Arch. Photogramm. Remote Sens. Spatial Inf. Sci.*, XLVIII-1/W2-2023, 1185–1190, <https://doi.org/10.5194/isprs-archives-XLVIII-1-W2-2023-1185-2023, 2023>

Leizea, I., Herrera, I., and Puerto, P. (2023). Calibration Procedure of a Multi-Camera System: Process Uncertainty Budget. *Sensors* 2023, 23, 589. <https://doi.org/10.3390/s23020589>

Lowe, D.G., (2004). Distinctive Features from Scale-Invariant Keypoints. *International Journal of Computer Vision* 60, 91-110 <https://doi.org/10.1023/B:VISI.0000029664.99615.94>

Luhmann, T. (2010). Close range photogrammetry for industrial applications. *ISPRS Journal of Photogrammetry and Remote Sensing*, Volume 65, Issue 6, 558-569. <https://doi.org/10.1016/j.isprsjprs.2010.06.003>

Luhmann, T., Fraser, C., & Maas, H-G. (2015). Sensor modelling and camera calibration for close-range photogrammetry. *ISPRS Journal of Photogrammetry and Remote Sensing*, Volume 115, 37-46. <https://doi.org/10.1016/j.isprsjprs.2015.10.006>

Mendikute, A., Yagüe-Fabra, J., Zatarain, M., Bertelsen, A., and Leizea, I. (2017). Self-Calibrated In-Process Photogrammetry for Large Raw Part Measurement and Alignment before Machining. *Sensors*, 2017, 17, 2066. <https://doi.org/10.3390/s17092066>

Moore, E. H. (1920). "On the reciprocal of the general algebraic matrix". *Bulletin of the American Mathematical Society*. 26 (9): 394–95. doi:10.1090/S0002-9904-1920-03322-7.

Penrose R. A generalized inverse for matrices. *Mathematical Proceedings of the Cambridge Philosophical Society*. 1955;51(3):406-413. doi:10.1017/S0305004100030401

Puerto, P., Heißelmann, D., Müller, S., and Mendikute, A. (2022). Methodology to Evaluate the Performance of Portable

Photogrammetry for Large-Volume Metrology. *Metrology* 2022, 2(3), 320-324. <https://doi.org/10.3390/metrology2030020>

Remondino, F. & Fraser, C. (2005). Digital camera calibration methods: considerations and comparisons. *ISPRS Volume XXXVI, Part 5*, 266-272

Sun, P., Lu, N., Dong, M., Yan, B., and Wang J. (2018). Simultaneous All-Parameters Calibration and Assessment of a Stereo Camera Pair Using a Scale Bar. *Sensors* 2018, 18(11), 3964. <https://doi.org/10.3390/s18113964>

Sun, P., Lu, N., Dong, M., Wang J. and Yan, B. (2019). Calibration and orientation of industrial online photogrammetry systems in situ. *The Journal of Engineering*, Volume 2019, Issue 23, 9137-9142 <https://doi.org/10.1049/joe.2018.9202>

Wang, Q., Zissler, N., and Holden, R. (2013). Evaluate error sources and uncertainty in large scale measurement systems. *Robotics and Computer-Integrated Manufacturing*. Volume 29, Issue I, 1-11. <https://doi.org/10.1016/j.rcim.2012.06.003>

<https://www.measure.com.au/metrology/laser-trackers/at403> last consulted on 27/03/2024.

<https://www.picoxr.com/it/products/pico4> last consulted on 27/03/2024.

<https://www.meta.com/it/en/quest/products/quest-2/> last consulted on 27/03/2024.

<https://www.vive.com/us/product/vive-xr-elite/overview/> last consulted on 27/03/2024.

<https://eshop.fujifilm-x.com/fujifilm-gfx100-ii.html> last consulted on 27/03/2024.